Magnetic Resonance Imaging 122 (2025) 110448

Contents lists available at ScienceDirect

Magnetic Resonance Imaging

journal homepage: www.elsevier.com/locate/mri

Qualitative and quantitative analysis of functional cardiac MRI using a novel compressed SENSE sequence with artificial intelligence image reconstruction

Konstantin Klein [a,*,1], Marcel Christian Langenbach [a,b,1], Lenhard Pennig [a], Thomas Schömig [a], Robert Terzis [a], Isabel Luisa Langenbach [a,b], David Maintz [a], Matej Gajzler [a], Kristina Sonnabend [a], Claas Philip Nähle [a,c]

[a] University Hospital Cologne, Cologne, Germany
[b] Cardiovascular Imaging Research Center, Massachusetts General Hospital, Boston, MA, USA
[c] Radiologische Allianz, Hamburg, Germany

ARTICLE INFO

Keywords:
Magnetic resonance imaging
Cardiac MRI
Artificial intelligence
Deep learning
Accelerated MRI scans

ABSTRACT

Background: To evaluate the feasibility of combining Compressed SENSE (CS) with a newly developed deep learning-based algorithm (CS-AI) using a Convolutional Neural Network to accelerate balanced steady-state free precession (bSSFP)-sequences for cardiac magnetic resonance imaging (MRI).

Methods: 30 healthy volunteers were examined prospectively with a 3 T MRI scanner. We acquired CINE bSSFP sequences for short axis (SA, multi-breath-hold) and four-chamber (4CH)-view of the heart. For each sequence, four different CS accelerations and CS-AI reconstructions with three different denoising parameters, CS-AI medium, CS-AI strong, and CS-AI complete, were used. Cardiac left ventricular (LV) function (i.e., ejection fraction, end-diastolic volume, end-systolic volume, and LV mass) was analyzed using the SA sequences in every CS factor and each AI level. Two readers, blinded to the acceleration and denoising levels, evaluated all sequences regarding image quality and artifacts using a 5-point Likert scale. Friedman and Dunn's multiple comparison tests were used for qualitative evaluation, ANOVA and Tukey Kramer test for quantitative metrics.

Results: Scan time could be decreased up to 57 % for the SA-Sequences and up to 56 % for the 4CH-Sequences compared to the clinically established sequences consisting of SA-CS3 and 4CH-CS2,5 (SA-CS3: 112 s vs. SA-CS6: 48 s; 4CH-CS2,5: 9 s vs. 4CH-CS5: 4 s, $p < 0.001$). LV-functional analysis was not compromised by using accelerated MRI sequences combined with CS-AI reconstructions (all $p > 0.05$). The image quality loss and artifact increase accompanying increasing acceleration levels could be entirely compensated by CS-AI post-processing, with the best results for image quality using the combination of the highest CS factor with strong AI (SA-CINE: Coef.:1.31, 95 %CI:1.05–1.58; 4CH-CINE: Coef.:1.18, 95 %CI:1.05–1.58; both $p < 0.001$), and with complete AI regarding the artifact score (SA-CINE: Coef.:1.33, 95 %CI:1.06–1.60; 4CH-CINE: Coef.:1.31, 95 % CI:0.86–1.77; both $p < 0.001$).

Conclusion: Combining CS sequences with AI-based image reconstruction for denoising significantly decreases scan time in cardiac imaging while upholding LV functional analysis accuracy and delivering stable outcomes for image quality and artifact reduction. This integration presents a promising advancement in cardiac MRI, promising improved efficiency without compromising diagnostic quality.

* Corresponding author.
E-mail addresses: konstantin.klein1@uk-koeln.de (K. Klein), mlangenbach@mgh.harvard.edu (M.C. Langenbach), lenhard.pennig@uk-koeln.de (L. Pennig), thomas.schoemig@uk-koeln.de (T. Schömig), robert.terzis@uk-koeln.de (R. Terzis), ILangenbach@mgh.harvard.edu (I.L. Langenbach), david.maintz@uk-koeln.de (D. Maintz), kristina.sonnabend@uk-koeln.de (K. Sonnabend), naehle@radiologische-allianz.de (C.P. Nähle).
[1] Contributed equally.

https://doi.org/10.1016/j.mri.2025.110448
Received 9 March 2025; Received in revised form 31 May 2025; Accepted 15 June 2025
Available online 19 June 2025

1. Introduction

Cardiac magnetic resonance imaging (MRI) is an essential diagnostic tool for assessing cardiac function, morphology, and tissue characteristics in various cardiovascular conditions, including ischemic heart disease, valvular heart disease, and cardiomyopathies [1,2]. However, traditional cardiac MRI (CMR) protocols often suffer from long acquisition times, primarily due to the need for high temporal and spatial resolution, multiple contrasts, and whole-heart coverage, exacerbated by respiratory and cardiac motion [3]. To address these challenges, advancements such as parallel imaging techniques like SENSE and GRAPPA have been introduced over the years, followed by more recent innovations like compressed sensing (CS) [4,5]. CS accelerates MRI acquisition by undersampling k-space, offering significant reductions in scan time. However, aggressive undersampling can compromise image quality by violating the Nyquist criterion, leading to artifacts such as blurring and aliasing [6].

While CS exploits the sparsity of images or their representations in mathematical transform domains for data recovery, the choice of reconstruction algorithm critically impacts image quality [7]. Recent developments have seen the integration of deep learning (DL)-based algorithms into MRI reconstruction processes, offering promising avenues for further acceleration and image enhancement. For instance, Pezzotti et al. introduced Adaptive-CS-Net, a novel deep learning-based algorithm, during the 2019 fastMRI challenge, demonstrating its efficiency in reconstructing undersampled MRI data with CS schemes [8,9]. This technology holds the potential for analyzing various anatomical areas and tissue types through expanded training datasets encompassing diverse anatomies, contrasts, and acceleration factors.

Despite these advancements, a notable research gap remains regarding the application of CS and DL-based reconstruction techniques, specifically in functional cardiac MRI. While these techniques have shown promise in other anatomical areas, their efficacy, reliability, and clinical relevance in cardiac MRI have yet to be investigated [10]. Addressing this gap could provide valuable insights into the feasibility and potential benefits of integrating these cutting-edge technologies into routine CMR protocols, offering clinicians enhanced diagnostic capabilities.

The study aimed to assess the feasibility and effectiveness of integrating CS with a newly developed DL algorithm, CS-AI, utilizing a convolutional neural network (CNN) to accelerate balanced steady-state free precession (bSSFP) sequences for CMR.

2. Material and methods

2.1. Study population

This prospective single-center study was performed on 30 healthy volunteers and was conducted in compliance with the ethical principles outlined in the 1964 Declaration of Helsinki and its subsequent amendments. The study received approval from the institutional review board (IRB no. 17–080) and was registered in the German Clinical Trials Register (DRKS00024156). Written informed consent was obtained from all participants. We did not include individuals presenting contraindications for the MRI examination (e.g., claustrophobia), known thoracic extraneous material with the potential to cause artifacts, and restricted ability to fulfill breath-hold maneuvers. Individuals were enrolled, and corresponding imaging data was acquired between January 2022 and December 2022.

2.2. MRI acquisition

All examinations were performed on the same 3.0 Tesla (T) MRI scanner (Ingenia 3.0 T, Philips Healthcare, Best, The Netherlands). For image acquisition, we used a dStream torso coil (receive coil, 8 channels) in combination with a posterior coil (receive coil, 16 channels). All individuals were placed in a head-first supine position. The operating technician trained the individuals in advance to perform breath-holding during the examination to ensure that the patient could cooperate accordingly. The MRI protocol included CINE bSSFP sequences for short-axis (SA, multi-breath-hold) and four-chamber (4CH) views of the heart. Detailed scan parameters are provided in **Supplemental Table S1**. Each sequence was acquired four times using varying CS factors (4CH: CS 2.5, CS 3, CS 4, CS 5; SA: CS 3, CS 4, CS 5, CS 6). Post-processing was conducted for each CS factor using three different, newly developed DL-based denoising algorithms (medium AI, strong AI, and complete AI vs. non-AI). In this context, denoising increases in a non-linear manner from medium through strong to complete.

2.3. Qualitative image analysis

All MRI scans were transferred as DICOM files to the local Picture Archiving and Communication System (PACS) for evaluation. Two experienced radiologists, each with over five years of experience, blinded to the used CS factor and the denoising level, independently evaluated all images. For qualitative analyses, images were rated regarding overall image quality using a 5-point Likert scale (1 = non-diagnostic, 2 = acceptable, 3 = moderate, 4 = good, 5 = excellent) and regarding artifacts (1 = severe artifacts/non-diagnostic, 2 = major artifacts/still diagnostic, 3 = minor artifacts, 4 = insignificant/slight artifacts, 5 = no artifacts). Both radiologists evaluated the images in consensus.

2.4. Quantitative image analysis

We performed a functional analysis of the left ventricular (LV) for quantitative analysis of the different CS factors and denoising levels. Therefore, we evaluated the SA CINE sequences in each CS level and denoising level. The evaluation was conducted using a standard clinical workstation and FDA-certified software package (IntelliSpace, Philips Healthcare, Best, The Netherlands). LV endocardial and epicardial borders were detected semi-automated, and LV contours were adjusted accordingly, if necessary, by the readers to ensure optimal consistency and precision. Papillary muscles and trabeculae were excluded from the LV mass during myocardial border drawing. We evaluated the following LV parameters: ejection fraction (EF), end-diastolic volume (EDV), end-systolic volume (ESV), and LV mass.

2.5. Statistical analysis

Data was collected in a computerized database (Excel®, Microsoft Corp.). Quantitative variables were described with mean and SD or median, minimum, and maximum qualitative variables with absolute and relative frequency (%). Categorical variables were compared using the Fisher exact test, and continuous variables were compared using the one-way ANOVA test for normal distribution or the Kruskal–Wallis *t*-test for asymmetric distribution. We used multilevel mixed-effects linear regression models to assess the influence of the CS factor and denoising level reconstructions, including interaction terms and clinical characteristics (age, sex, BMI). CS2.5, combined with non-AI reconstruction, was used as the reference for evaluating the sequences. In the essentially exploratory analysis, p values ≤ 0.05 were considered statistically significant. Statistical analyses were performed using Stata (Stata 17, Stata Corp.) and GraphPad Prism version 9.0.1 (GraphPad Software, San Diego, California, USA).

3. Results

The MRI was performed on 30 healthy individuals (19 females (63.3 %)) with a median age of 31 years (range: 23–63 years), a mean weight of 73.3 kg (±12.7 kg), and a mean height of 173 cm (±9 cm). All examinations were performed successfully without any interruptions or abortions (Table 1). Scan time could be decreased up to 57 % for the SA-

Table 1
Clinical characteristics of included patients.

Clinical Characteristics	Values, *mean ± SD, median (range), n (%)*
Age, years	31 (23–63)
Female	19 (63.3)
Weight, kg	73.3 ± 12.7
Height, cm	173 ± 9
BMI	24.0 ± 2.5
Ejection fraction, %	68.9 ± 4.8
End-systolic volume, ml	38.9 ± 10.1
End-diastolic volume, ml	124.8 ± 21.9
End-diastolic wall mass, g	88.6 ± 14.8

BMI, body mass index; SD, standard deviation.

Sequences and up to 56 % for the 4CH-Sequences compared to the clinically established sequences consisting of SA-CS3 and 4CH-CS2,5 (SA: CS3: 112 s, CS4: 80s, CS5: 60s, CS6: 48 s; 4CH: CS2,5: 9 s, CS3: 7 s, CS4: 6 s, CS5: 4 s; all $p < 0.001$). For the short-axis acquisition, the number of required breath-holds could be reduced by up to 50 % (CS3 vs. CS6).

3.1. Qualitative assessment of the image quality

In the SA CINE sequences, the CS factor and the level of AI reconstructions exerted discernible influences on image quality. Notably, the CS factor significantly decreased overall image quality (CS3: 4.6 vs. CS4: 4.3 vs. CS5: 4.1 vs. CS6: 3.8, $p < 0.001$). The choice of AI reconstruction improved the image quality significantly (non-AI: 3.4 vs. AI: 4.2 vs. strong AI: 4.8 vs. complete AI: 4.4, $p < 0.001$) (**Supplemental Table S2**).

The multivariable regression analysis unveiled that higher CS factors were associated with a decrement in image quality compared to the reference CS3 (CS4: -0.3, CS5: -0.6, CS6: −0.8, all $p < 0.001$). Conversely, elevated levels of AI reconstruction corresponded to enhanced image quality, with the most notable improvement observed at the strong AI level (AI: +0.8, strong AI: +1.4, complete AI: +1.0, all $p < 0.001$). These coefficients remained constant and significant after adjusting for age, sex, and BMI. Images demonstrating the three different denoising levels vs. non-AI are shown in Fig. 1 and Fig. 2**.**

The mixed regression analysis demonstrated that employing CS level 5 with strong AI reconstruction yielded significantly superior results compared to the standard CS 3 and non-AI combination (Coef. +1.3, $p < 0.001$). This finding persisted in the adjusted model. Refer to Table 2 for comprehensive details.

Similar trends were observed in the 4CH CINE images. Analogous to SA CINE, higher CS factors were associated with notable declines in image quality (CS2.5: 4.2 vs. CS4: 4.1 vs. CS5: 3.4 vs. CS6: 3.3, $p < 0.001$). Conversely, AI reconstruction levels significantly enhanced image quality (non-AI: 3.0 vs. AI: 3.5 vs. strong AI: 4.4 vs. complete AI: 4.0, $p < 0.001$).

Regression analysis indicated that higher CS factors, particularly CS4 and CS5, were linked with diminished image quality compared to the reference CS2.5 (CS3: −0.1, $p = 0.17$; CS4: -0.8, CS5: −0.9; both $p < 0.001$). Conversely, strong AI reconstruction consistently improved image quality, with the most notable gains observed at the strong AI level (AI: +0.5, strong AI: +1.4, complete AI: +1.0; all $p < 0.001$). Mixed regression analysis underscored that employing CS level 4 alongside strong AI reconstruction significantly outperformed the standard CS 3 and non-AI combination (+1.2, $p < 0.001$). These findings were consistent and robust across the adjusted model (Table 2).

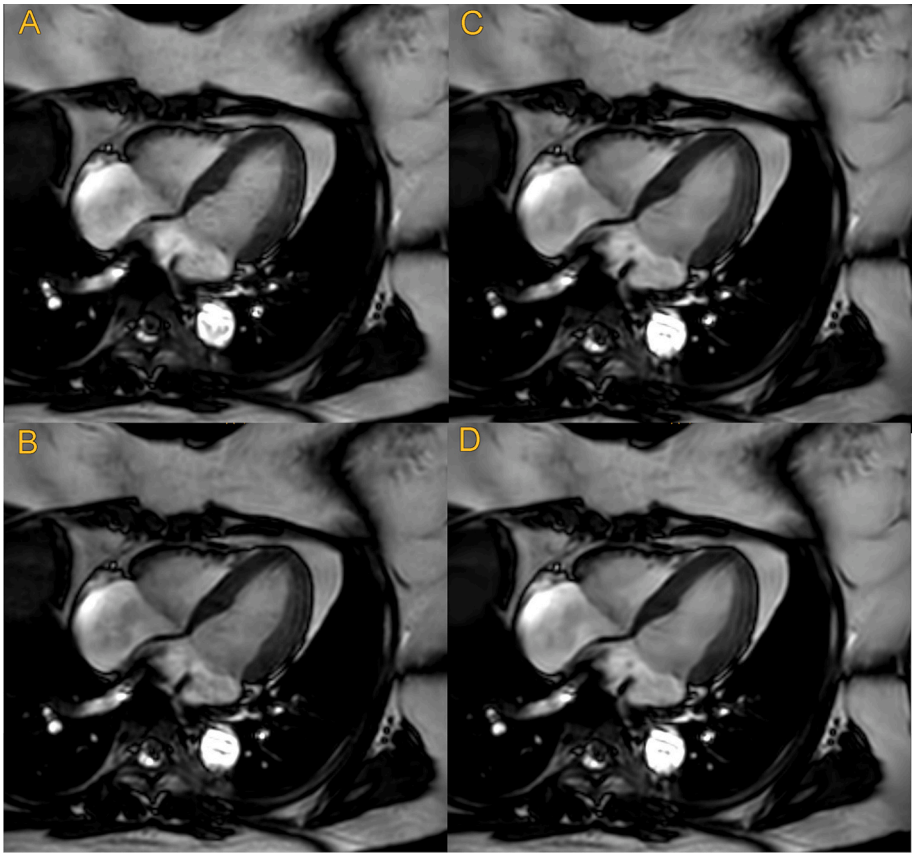

Fig. 1. 4-CH view at the highest CS level (CS 5) and 3 ascending denoising levels using the DL-denoising algorithm. A: non-AI, B: CS-AI medium, C: CS-AI strong, D: CS-AI complete.
4CH, four-chamber; AI, artificial intelligence; CS, compressed sense; DL, deep learning.

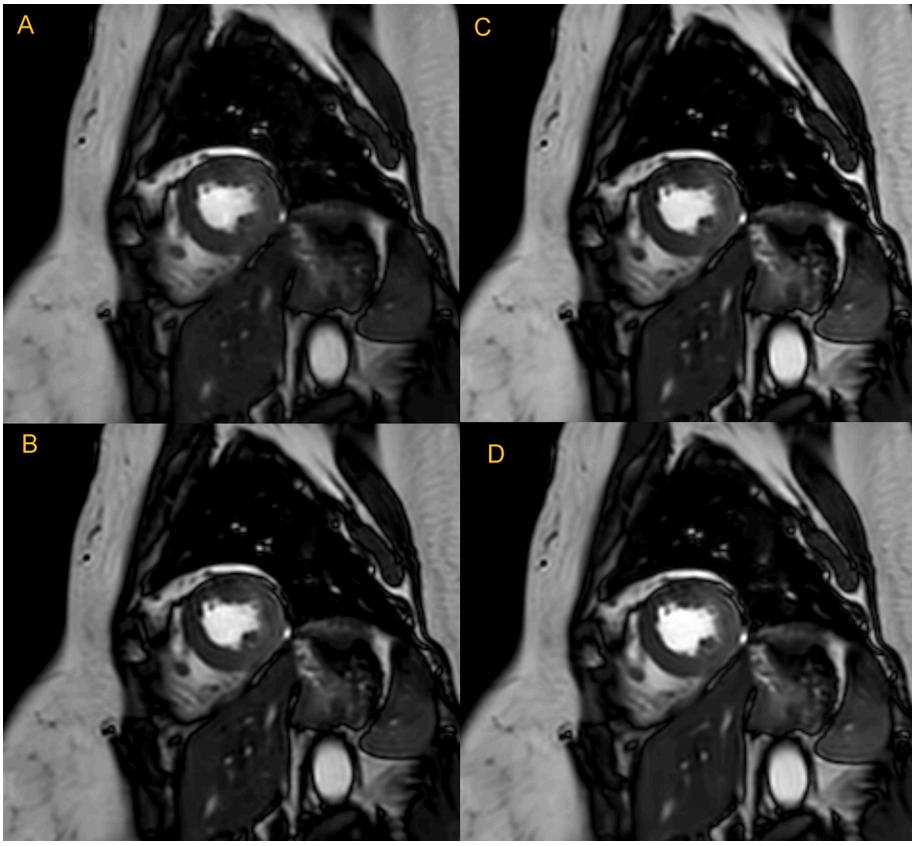

Fig. 2. SA view at the highest CS level (CS 6) and 3 ascending denoising levels using the DL-denoising algorithm. A: non-AI, B: CS-AI medium, C: CS-AI strong, D: CS-AI complete.
SA, short axis; AI, artificial intelligence; CS, compressed sense; DL, deep learning.

3.2. Artifact assessment

For both SA CINE and 4CH CINE sequences, the artifact score exhibited significant variations based on the chosen parameters. A higher CS factor corresponded to lower artifact scores, with optimal scores observed for CS3 and CS2.5, respectively (SA CINE: CS3: 4.7 vs. CS4: 4.6 vs. CS5: 4.2 vs. CS6: 4.0, $p < 0.001$; 4CH CINE: CS2.5: 4.3 vs. CS3: 4.1 vs. CS4: 3.3 vs. CS5: 3.2, $p < 0.001$). Conversely, employing stronger denoising reconstructions resulted in higher artifact scores, indicative of fewer artifacts, with the most favorable outcomes observed with complete AI reconstruction (SA CINE: non-AI: 3.6 vs. AI: 4.2 vs. strong AI: 4.8 vs. complete AI: 4.9, $p < 0.001$; 4CH CINE: non-AI: 2.9 vs. AI: 3.5 vs. strong AI: 4.1 vs. complete AI: 4.4, $p < 0.001$).

Regression analysis further elucidated that higher CS factors were associated with decreased artifact occurrence in both sequences, with the lowest scores recorded for CS6 and CS5, respectively (SA CINE: CS6–0.7, $p < 0.001$; 4CH CINE: CS5–1.0, $p < 0.001$). These effects remained consistent following adjustment for age, sex, and BMI. Furthermore, utilizing the most robust denoising algorithm, complete AI, led to significant artifact reduction, with increases of +1.4 for SA CINE and + 1.5 for 4CH CINE (both $p < 0.001$), a trend that persisted post-adjustment.

Mixed regression analysis underscored that combining CS6 (SA CINE) and CS5 (4CH CINE) with complete AI reconstruction yielded markedly superior results compared to the standard CS3/CS2.5 and non-AI combination (both +1.3; both $p < 0.001$). These findings retained significance and consistency in the adjusted model. Refer to Table 3 for a comprehensive overview of artifact assessments.

3.3. Quantitative analysis

The SA CINE CS3 non-AI sequence, widely employed in clinical practice, serves as the benchmark for functional analysis evaluation. Detailed results of the analysis can be found in **Supplemental Table S3**. Quantitative assessment reveals that none of the reconstruction algorithms nor acceleration factors demonstrate significant deviations in determining key functional parameters: ejection fraction (EF) ($\boldsymbol{p} = 0.95$ and $\boldsymbol{p} = 0.93$, respectively), end-diastolic volume (EDV) ($\boldsymbol{p} = 0.43$ and $\boldsymbol{p} = 0.96$, respectively), end-systolic volume (ESV) ($\boldsymbol{p} = 0.34$ and $\boldsymbol{p} = 0.97$, respectively), and left ventricular (LV) mass ($\boldsymbol{p} = 0.67$ and $\boldsymbol{p} = 0.74$, respectively) when compared to the reference scan. Furthermore, regression analysis indicates no significant associations between the reconstruction algorithms, acceleration factors, and the evaluated functional parameters. Refer to Table 4 for comprehensive details regarding these associations.

4. Discussion

Our findings showed that CS acquisition methods can significantly accelerate cardiac MRI. With increasing acceleration, the image quality was compromised, and images were more prone to artifacts. This could be mitigated by applying AI-based denoising algorithms for post-processing, ensuring that even at increased acceleration factors, a diagnostic image quality is maintained, superior to reconstructions without postprocessing.

The persistent challenge of slow image acquisition in MRI has long been recognized [11,12]. Lengthy scan times contribute to several drawbacks, including motion artifacts, difficulties in patient cooperation for breath-hold commands, and increased costs due to low patient throughput. In today's healthcare landscape, the demand for expedited

Table 2
Mixed regression analysis to investigate the association of the CS factor and the denoising algorithm with the image quality.

	SA CINE				4CH CINE		
	Coef.	*p*-value	95 % Conf. Interval		Coef.	p-value	95 % Conf. Interval
CS factor				**CS factor**			
CS3	Ref.			CS2.5	Ref.		
CS4	−0.53	**<0.001**	−0.72 to −0.35	CS3	−0.28	**0.022**	−0.52 to −0.04
CS5	−0.92	**<0.001**	−1.10 to −0.73	CS4	−1.25	**<0.001**	−1.49 to −1.01
CS6	−1.45	**<0.001**	−1.64 to −1.26	CS5	−1.63	**<0.001**	−1.88 to −1.39
Denoising algorithm				**Denoising algorithm**			
Non-AI	Ref.			Non AI	Ref.		
AI	0.58	**<0.001**	0.40–0.77	AI	0.17	0.18	−0.08–0.41
Strong AI	0.77	**<0.001**	0.58–0.95	Strong AI	0.85	**<0.001**	0.61–1.09
Complete AI	0.67	**<0.001**	0.48–0.85	Complete AI	0.52	**<0.001**	0.27–0.75
CS factor/Denoising algorithm				**CS factor/Denoising algorithm**			
CS3/Non-AI	Ref.			CS2.5/Non AI	Ref.		
CS4/AI	0.15	0.26	−0.11–0.41	CS3/AI	0.23	0.18	−0.11–0.58
CS5/AI	0.15	0.26	−0.11–0.41	CS4/AI	0.50	**0.004**	0.15–0.84
CS6/AI	0.50	**<0.001**	0.24–0.76	CS5/AI	0.77	**<0.001**	0.42–1.11
CS4/Strong AI	0.53	**<0.001**	0.27–0.79	CS3/Strong AI	0.28	0.11	−0.06–0.63
CS5/Strong AI	0.81	**<0.001**	0.55–1.08	CS4/Strong AI	0.70	**<0.001**	0.35–1.04
CS6/Strong AI	1.31	**<0.001**	1.05–1.58	CS5/Strong AI	1.18	**<0.001**	0.83–1.53
CS4/Complete AI	0.23	0.08	−0.03–0.50	CS3/Complete AI	0.25	0.15	−0.09–0.59
CS5/Complete AI	0.35	**0.009**	0.09–0.61	CS4/Complete AI	0.72	**<0.001**	0.37–1.06
CS6/Complete AI	0.68	**<0.001**	0.42–0.94	CS5/Complete AI	1.07	**<0.001**	0.72–1.41
Clinical Characteristics				**Clinical Characteristics**			
Age	0.00	0.20	−0.00–0.00	Age	0.00	0.44	−0.00–0.01
Sex *(male)*	0.00	0.90	−0.01–0.01	Sex *(male)*	0.00	0.17	−0.03–0.01
BMI	−0.03	0.40	−0.10–0.04	BMI	−0.03	**0.011**	−0.20 to −0.03

4CH, four-chamber; AI, artificial intelligence; BMI, body mass index; Coef., coefficient; CS, compressed sense; SA, short axis.

Table 3
Mixed regression analysis to investigate the association of the CS factor and the denoising algorithm with the artifact score.

	SA CINE				4CH CINE		
	Coef.	p-value	95 % Conf. Interval		Coef.	p-value	95 % Conf. Interval
CS factor				**CS factor**			
CS3	Ref.			CS2.5	Ref.		
CS4	−0.17	0.09	−0.36–0.25	CS3	−0.53	**0.001**	−0.85 to −0.21
CS5	−0.98	**<0.001**	−1.17 to −0.79	CS4	−1.35	**<0.001**	−1.67 to −1.02
CS6	−1.35	**<0.001**	−1.5 to −1.56	CS5	−1.68	**<0.001**	−2.00 to −1.36
Denoising algorithm				**Denoising algorithm**			
Non-AI	Ref.			Non AI			
AI	0.62	**<0.001**	0.43–0.81	AI	0.40	**0.015**	0.78–0.72
Strong AI	0.72	**<0.001**	0.53–0.91	Strong AI	0.68	**<0.001**	0.36–1.00
Complete AI	0.75	**<0.001**	0.55–0.94	Complete AI	0.75	**<0.001**	0.42–1.07
CS factor/Denoising algorithm				**CS factor/Denoising algorithm**			
CS3/Non-AI	Ref.			CS2.5/Non AI	Ref.		
CS4/AI	−0.13	0.34	−0.40–0.14	CS3/AI	0.15	**0.015**	0.08–0.72
CS5/AI	0.10	0.47	−0.17–0.37	CS4/AI	0.21	0.93	−0.23–0.67
CS6/AI	0.22	0.12	−0.05–0.49	CS5/AI	0.40	0.09	−0.05–0.85
CS4/Strong AI	0.18	0.19	−0.09–0.45	CS3/Strong AI	0.52	**0.026**	0.06–0.97
CS5/Strong AI	0.81	**<0.001**	0.55–1.08	CS4/Strong AI	0.58	**0.012**	0.12–1.04
CS6/Strong AI	0.93	**<0.001**	0.66–1.20	CS5/Strong AI	0.88	**<0.001**	0.42–1.34
CS4/Complete AI	0.18	0.19	−0.09–0.45	CS3/Complete AI	0.75	0.52	0.30–1.20
CS5/Complete AI	0.97	**<0.001**	0.70–1.23	CS4/Complete AI	0.88	**<0.001**	0.42–1.34
CS6/Complete AI	1.33	**<0.001**	1.06–1.60	CS5/Complete AI	1.31	**<0.001**	0.86–1.77
Clinical Characteristics				**Clinical Characteristics**			
Age	0.00	0.19	−0.00–0.01	Age	0.01	**0.009**	0.00–0.01
Sex *(male)*	0.00	0.33	−0.01–0.02	Sex *(male)*	−0.01	0.33	−0.03–0.01
BMI	−0.03	0.06	−0.14–0.00	BMI	−0.15	**0.015**	−0.27 to −0.03

4CH, four-chamber; AI, artificial intelligence; BMI, body mass index; Coef., coefficient; CS, compressed sense; SA, short axis.

Table 4
Logistic regression analysis to investigate the association of the CS factor and the denoising algorithm with the LV functional assessment.

	Ejection fraction, *%*			End-diastolic volume, *ml*			End-systolic volume, *ml*			Left ventricular mass, *g*		
	Coef.	p-value	95 % Conf. Interval	Coef.	p-value	95 % Conf. Interval	Coef.	*p*-value	95 % Conf. Interval	Coef.	*p*-value	95 % Conf. Interval
CS factor												
CS3	Ref.			Ref.			Ref.			Ref.		
CS4	0.31	0.60	−0.84–1.46	−1.34	0.56	−6.14–3.46	−0.90	0.45	−3.22–1.42	0.61	0.65	−1.99–3.20
CS5	0.40	0.50	−0.76–1.54	−3.81	0.12	−8.62–0.99	−2.21	0.06	−4.52–0.11	0.69	0.61	−1.91–3.28
CS6	0.37	0.53	0.78–1.52	−3.70	0.13	−8.48–1.12	−1.50	0.20	−3.82–0.82	−1.24	0.35	−3.84–1.36
Denoising algorithm												
Non-AI	Ref.			Ref.			Ref.			Ref.		
AI	−0.23	0.70	−1.37–0.92	−0.91	0.71	−5.72–3.90	0.12	0.92	−2.19–2.44	−1.26	0.34	−3.86–1.34
Strong AI	−0.17	0.98	−1.17–1.13	−0.94	0.70	−5.74–3.87	−0.11	0.92	−2.43–2.20	−1.56	0.24	−4.16–1.03
Complete AI	0.11	0.85	−1.04–1.25	−1.80	0.47	−6.57–3.04	−0.46	0.70	−2.77–1.86	−1.71	0.20	−4.30–0.89
Clinical Characteristics												
Age	0.11	**<0.001**	0.07–0.15	−0.07	0.45	−0.24–0.11	−0.14	**0.001**	−0.23 to −0.06	−0.13	**0.005**	−0.23 to −0.04
Sex *(male)*	0.47	**<0.001**	0.31–0.63	0.49	0.16	−0.20–1.17	−0.47	**0.005**	−0.80 to −0.14	1.11	**<0.001**	0.74–1.48
BMI	−1.61	**<0.001**	−2.50 to −0.73	22.32	**<0.001**	18.62–26.02	9.12	**<0.001**	7.33–10.90	21.46	**<0.001**	19.45–23.46

AI, artificial intelligence; BMI, body mass index; Coef., coefficient; CS, compressed sense.

MRI examinations without sacrificing image quality has become increasingly pressing, with the economic implications of prolonged scan times resulting in reduced patient throughput and higher examination costs [12]. Moreover, motion artifacts frequently compromise image quality, as maintaining absolute stillness for extended periods during scanning is challenging, even for healthy individuals. Reducing examination times in clinical practice increases MRI productivity and enhances patient comfort during the procedure. This improved comfort fosters better image quality by promoting patient compliance and reducing the likelihood of motion artifacts [13].

Several recent studies have similarly demonstrated that deep learning–based reconstruction techniques can enable substantial acceleration of cardiac MRI without compromising diagnostic accuracy. For instance, Masutani et al. reported that that deep learning methods (CNNs) can significantly enhance the image quality of cardiac MRI scans through super-resolution, by more effectively restoring high-frequency image details compared to traditional upscaling methods such as bicubic interpolation or zero padding - without compromising the accuracy of functional measurements such as left ventricular volumes [12].

Furthermore, Kuestner et al. showed that key functional parameters such as ejection fraction and stroke volume remained consistent across accelerated and conventional sequences, highlighting the clinical applicability of these techniques [13]. These findings support our observation that CS-AI allows for faster acquisition while maintaining quantitative reliability.

In our study the trend showed a significant improvement in image quality at acceleration factors of CS2.5, CS3, and CS4 using the CS-AI algorithm. This suggests that using an AI-based reconstruction algorithm allows better exploitation of the under-sampled data than the conventional CS reconstruction algorithm. Thus, using strong and complete denoising in the 4CH CINE and SA CINE sequences, the CS-AI algorithm allows strong acceleration up to a factor of CS6.

The image quality remains consistent and even improves up to a factor of CS4 with moderate acceleration compared to the reference scan. However, a difference in image quality was observed within these two denoising levels. The CS-AI-Strong reconstruction algorithm provides the overall best image quality. The slightly lower rating of images from the CS-AI-Complete reconstruction algorithm may be due to the strong denoising. Image information may be lost due to the need for more consistency checks. Additionally, heavily denoised images have a soft appearance, which may be unfamiliar and result in lower ratings by radiologists. The CS-AI-Strong algorithm is recommended for acquiring CINE bSSFP cardiac MRI images based on subjective analysis.

Objective analysis showed that all acceleration factors and reconstruction algorithms are suitable for functional analysis. There were no significant differences in results between conventional and CS-AI images for all four evaluated parameters. This allows using CS-AI algorithms in CINE imaging for left ventricular functional analysis without the risk of significantly different measurements compared to the reference scan. This study has shown that higher acceleration and the new CS-AI reconstruction method mainly affect the subjective image appearance and the occurrence of artifacts, with no significant effect on objective, quantitative parameters, such as those used for functional analysis. This may be due to the unfamiliar appearance of the images resulting from different denoising parameters. A higher denoising level provides much softer images and, therefore, a different subjective perception of the image's appearance. While the functional analysis is a standardized procedure evaluated with the software, it may be advantageous to introduce CS-AI images in addition to clinical standard protocols when implementing CS-AI in the clinical workflow. This approach would allow radiologists to understand CS-AI images better and determine when they should be used.

Overall, the CS-AI algorithm allows the acquisition of more heavily undersampled data, which can be utilized in various ways in clinical practice. On the one hand, scan time can be shortened, and patient throughput can be increased by heavy undersampling. On the other hand, the gained scan time can be used for additional sequences or higher spatial resolution.

Scan time could be decreased up to 57 % for the SA-Sequences and up to 56 % for the 4CH-Sequences compared to the clinically established sequences (SA-CS3:112 s vs SA-CS6: 48 s; 4CH-CS2,5: 9 s vs. 4CH-CS5: 4 s) (Table 5). For the short-axis sequence, it is important to mention that with higher acceleration factors, more slices could be acquired per breath-hold, which significantly reduced the number of required breath-holds. When comparing the lowest and highest acceleration factors in the short-axis acquisition, 15 slices were acquired within 8 × 14 s (CS acceleration factor 3), compared to 4 × 20 s (CS acceleration factor 6),

Table 5
Scan time in seconds for 4CH CINE and SA CINE depending on each CS level.

	CS 2,5	CS 3	CS 4	CS 5	CS 6
4CH CINE	9 s	7 s	6 s	4 s	/
SA CINE	/	112 s	80s	60s	48 s

4CH, four-chamber; CS, compressed sense; SA, short axis.

which in this case corresponds to a halving of the number of breath-holds. The reference protocol consists of sequences applied in clinical practice with a total scan duration of 121 s. A protocol with moderate acceleration (55 s) consisting of 4CH CINE CS3 and SA CINE CS6 sequences offers higher acceleration and significantly improves image quality through CS-AI reconstructions. The last scenario includes sequences with the highest acceleration factors (4CH CINE CS 5 and SA CINE CS6) and constant image quality with a scan duration of 52 s. The AI denoising algorithms achieved a 55 % reduction in scan time (moderate protocol) and a significant improvement in image quality. A further reduction in total acquisition time of 57 % still provides images with acceptable diagnostic image quality at maximum acceleration.

Reducing scan time was also reported in a study by Foreman et al. in 2022. The impact of CS-AI on accelerating ankle MRI was evaluated in 30 patients. The protocol included axial T2 TSE, T2 TSE HR, coronal T1 TSE, coronal PD TSE, and sagittal PD TSE sequences. The results show that acquisition times with CS-AI can be reduced by 47 % compared to CS without compromising the diagnostic image quality [14].

4.1. Limitations

However, this study has some limitations. One disadvantage of the new AI denoising method is the reconstruction time. While the reconstruction of the CS method is almost instant, the reconstruction of all the data used here took about 30 min per subject, meaning a reconstruction time of approximately 7.5 min per sequence. This could lead to delays and reduce the time advantage. In this context, it should be noted that both the algorithm and the hardware were investigational tools and not commercially available products at the time of the study. We assume that with optimized hardware, an instantaneous reconstruction could be achieved.

We investigated a relatively small sample size of healthy individuals based on the pilot character of this trial. A future evaluation of a patient population is desirable, particularly with the DL-based reconstruction algorithms. It must be verified that the denoising algorithm's application might impact the pathologies' detectability. We expect comparable results since the algorithm was trained on data with and without pathological findings.

Furthermore, only the DL-based algorithm's application on the CMR protocol's CINE sequences was analyzed. A comprehensive analysis of all relevant sequences for CMR would be beneficial in fully exploiting the possibilities and limitations of the algorithm.

Due to the rapid development in MRI and initial promising results regarding the application of DL-based reconstruction algorithms in preclinical or clinical settings, it remains to be explored how the significance of AI in cardiovascular MRI will develop in the future. AI-based algorithms hold the potential to replace further steps in MRI acquisition and post-processing in the future, leading to even higher accelerations, artifact reduction, higher resolution, or automated evaluations such as functional analysis.

5. Conclusion

Regarding image quality, denoising using the AI-strong algorithm seems particularly recommendable, as the subjective overall image impression decreases with AI-complete. When it comes to reducing artifacts, the AI-complete algorithm would be preferable. Whether the AI-strong or the AI-complete algorithm should be used to post-process the accelerated sequences is ultimately a matter of user-specific taste. Still, both algorithms deliver excellent results regarding image quality and artifacts with only minor differences. The results of the LV-functional analysis remain unaffected by the choice of the CS level and denoising algorithm.

CRediT authorship contribution statement

Klein Konstantin: Writing – original draft, Data curation. **Langenbach Marcel Christian:** Supervision, Formal analysis. **Pennig Lenhard:** Supervision. **Schömig Thomas:** Data curation. **Terzis Robert:** Validation. **Langenbach Isabel Luisa:** Data curation. **Maintz David:** Supervision. **Gajzler Matej:** Investigation. **Sonnabend Kristina:** Formal analysis. **Nähle Claas Philip:** Supervision.

Appendix A. Supplementary data

Supplementary data to this article can be found online at https://doi.org/10.1016/j.mri.2025.110448.

References

[1] Busse A, et al. Cardiac MRI—Update 2020. Radiologe 2020;60:33–40.
[2] Bustin A, Fuin N, Botnar RM, Prieto C. From compressed-sensing to artificial intelligence-based cardiac MRI reconstruction. Front Cardiovasc Med 2020;7.
[3] Zhao Y, Peng C, Wang S, Liang X, Meng X. The feasibility investigation of AI -assisted compressed sensing in kidney MR imaging: an ultra-fast T2WI imaging technology. BMC Med Imaging 2022;22:119.
[4] Donoho DL. Compressed sensing. IEEE Trans Inf Theory 2006;52:1289–306.
[5] Lustig M, Donoho D, Pauly JM. Sparse MRI: the application of compressed sensing for rapid MR imaging. Magn Reson Med 2007;58:1182–95.
[6] Iuga AI, et al. A deep learning-based reconstruction approach for accelerated magnetic resonance image of the knee with compressed sense: evaluation in healthy volunteers. Br J Radiol 2023;96.
[7] Safari M, Eidex Z, Chang C-W, Qiu RLJ, Yang X. Advancing MRI reconstruction: a systematic review of deep learning and compressed sensing integration. 2025.
[8] Pezzotti N, et al. An adaptive intelligence algorithm for undersampled knee MRI reconstruction. IEEE Access 2020;8:204825–38.
[9] Pezzotti N, et al. Adaptive-CS-Net: FastMRI with adaptive intelligence. *ArXiv* arXiv: 1912.12259. 2019.
[10] Runge VM, Richter JK, Heverhagen JT. Speed in clinical magnetic resonance. Invest Radiol 2017;52:1–17.
[11] Zhang Q, et al. Improving the efficiency and accuracy of cardiovascular magnetic resonance with artificial intelligence—review of evidence and proposition of a roadmap to clinical translation. J Cardiovasc Magn Reson 2024;26:101051.
[12] Masutani EM, Bahrami N, Hsiao A. Deep learning single-frame and multiframe super-resolution for cardiac MRI. Radiology 2020;295:552.
[13] Küstner T, et al. CINENet: deep learning-based 3D cardiac CINE MRI reconstruction with multi-coil complex-valued 4D spatio-temporal convolutions. Sci Rep 2020;10: 1–13. 2020 10:1.
[14] Foreman SC, et al. Deep learning-based acceleration of compressed sense MR imaging of the ankle. Eur Radiol 2022;32:8376–85.